Case Studies in Chemical and Environmental Engineering 11 (2025) 101195

Contents lists available at ScienceDirect

Case Studies in Chemical and Environmental Engineering

journal homepage: www.sciencedirect.com/journal/case-studies-in-chemical-and-environmental-engineering

Case Report

Synthesis and investigation of the applicability of Fe_3O_4/ZnO nanoparticles as a basis for hyperthermic studies

Kamila B. Kaliyekperova [a,b], Vyacheslav S. Rusakov [c], Artem L. Kozlovskiy [a,b,*], Maxim S. Fadeev [c], Dmitriy I. Shlimas [a,b], Maxim V. Zdorovets [a,b]

[a] Engineering Profile Laboratory, L.N. Gumilyov Eurasian National University, Nur-Sultan, 010008, Kazakhstan
[b] Laboratory of Solid State Physics, The Institute of Nuclear Physics, Almaty, 050032, Kazakhstan
[c] M.V. Lomonosov Moscow State University, 119991, Moscow, Russia

ARTICLE INFO

Keywords:
$Fe_2O_3/ZnFe_2O_4$ nanoparticles
Magnetic materials
Hyperthermia
Phase transformations
Magnetite

ABSTRACT

Ferrimagnetic nanoparticles, which are compounds of iron oxide with other types of metal oxides, are one of the promising types of nanoparticles among a wide variety. Interest in this type of nanostructures is primarily due to the great prospects for their use in biomedical applications, targeted drug delivery, alongside hyperthermia and magnetic resonance therapy. The relevance of the research consists in obtaining new knowledge in the field of research of phase transformations in ferritic Fe_3O_4/ZnO nanoparticles under variation of synthesis conditions, alongside assessing their practical application in comparison with literature data, and determining the limits of applicability in hyperthermia. The key result of this study is to evaluate the effectiveness of using Fe_3O_4/ZnO nanoparticles, as well as determining the influence of thermal annealing conditions on the phase transformation processes in nanoparticles. According to X-ray phase analysis data, the dynamics of phase transformations in Fe_3O_4/ZnO nanoparticles contingent upon the thermal annealing temperature was established. These phase transformations can be written in the following form: $Fe_3O_4/ZnO \rightarrow Fe_2O_3/ZnO \rightarrow Fe_2O_3/ZnFe_2O_4 \rightarrow ZnFe_2O_4/ZnO$. During the studies, it was found that the formation of the $ZnFe_2O_4$ phase leads not only to the heating rate growth, but also to the formation of a linear dependence of the change in the solution temperature on the time of exposure to an alternating magnetic field.

1. Introduction

Today, one of the promising areas of research in the field of materials science is the production of various types of nanostructures, interest in which is due to the great possibilities of their practical application in various fields, ranging from microelectronics, biomedicine, sensors, photocatalysis, etc. [1–3]. This interest is primarily due to the variety of possibilities for obtaining different types of nanoparticles, both in elemental and phase composition, and geometry, the variation of which occurs as a result of changing synthesis conditions or subsequent modification. At the same time, in recent years, much attention has been paid to the possibilities of obtaining composite nanostructures, using the simplest and cheapest methods for their preparation [4,5]. This is primarily due to the need, in most cases, for a transition from laboratory testing of the applicability of nanoparticles to industrial testing, with the aim of introducing into production and scaling up the proposed technological solutions. The search for simple methods for producing nanoparticles, especially composite ones, is driven by the fact that when creating technology for their scaling, complex production processes are difficult to reproduce outside laboratory conditions, which require compliance with many factors, including the use of expensive chemical reagents, time-consuming and labor-intensive processes of creation and subsequent modification, etc. Also, an important factor that must be taken into account when scaling the technology for the reproduction of composite nanoparticles for industrial production is the repeatability and stability of the structural, morphological, and most importantly, the phase composition of the resulting composite nanoparticles, on which most of the characteristics that are key factors in their use depend [6–10].

Also, in addition to searching for opportunities to scale technological solutions in the search for the creation of composite nanoparticles, great attention should be paid to fundamental aspects related to the study of the relationship of conditions and methods of production with changes in structural, conductive or magnetic characteristics, phase composition,

* Corresponding author. Engineering Profile Laboratory, L.N. Gumilyov Eurasian National University, Nur-Sultan, 010008, Kazakhstan.
E-mail address: kozlovskiy.a@inp.kz (A.L. Kozlovskiy).

https://doi.org/10.1016/j.cscee.2025.101195
Received 8 February 2025; Received in revised form 17 March 2025; Accepted 17 March 2025
Available online 19 March 2025
2666-0164/© 2025 The Authors. Published by Elsevier Ltd. This is an open access article under the CC BY-NC-ND license (http://creativecommons.org/licenses/by-nc-nd/4.0/).

etc. Interest in this area of research is primarily aimed at studying the properties of nanoparticles when their sizes change, as well as the transition from macro-sized to nano-sized parameters, which can have a significant impact on alterations in the properties of materials, the occurrence of size effects affecting conductivity, toxicity, corrosion resistance, etc. [11–15]. Moreover, for composite nanostructures, in which, as a rule, several phases are combined, and variation in synthesis conditions allows one to vary the phase composition due to phase transformations or polymorphic transformations, the fundamental study of the properties of nanoparticles is a very important aspect in their practical application.

Among the variety of different types of composite nanoparticles, a special place is occupied by ferrite structures, which are based on compounds of iron oxide with various oxide compounds, such as oxide of nickel, cobalt, zinc, copper, cadmium, etc. Interest in ferrite nanoparticles is primarily due to the possibility of combining the structural and magnetic properties of various oxides, as well as the ease of obtaining iron oxides, which are the basis for these structures [16–19]. Typically, iron oxide nanoparticles are prepared using chemical precipitation methods from various aqueous solutions, which produce stable, mostly monodisperse iron oxide nanoparticles in the form of magnetite or hematite, the two most common iron oxide phases found in nature. At the same time, the use of the simplest procedures for modification, in particular, thermal annealing in the temperature range from 100 to 600–700 °C, makes it possible to initiate phase transformations such as Fe_3O_4 – magnetite → Fe_2O_3 – hematite, without significant changes in the size of nanoparticles. Moreover, an alteration in the phase composition of iron-containing nanoparticles primarily has a significant impact on their conductive properties, as well as magnetic characteristics, the change of which must be considered in the further practical use of nanoparticles [20].

Also, interest in ferrite nanoparticles is due to their low toxicity (and in most cases its complete absence) and high biocompatibility, which allows the use of these ferrite nanoparticles in biomedicine, as a basis for targeted delivery of drugs, hyperthermic studies, etc. The use of magnetic nanoparticles in biomedicine has been actively studied in recent years due to the possibility of using these particles not only as contrast fluids for MRI, but also in the case of considering their applicability as drug carriers for which "core-shell" type particles are used [21], where great interest is paid to the possibilities of combining a magnetic particle used as a core, coated with various polymer [22] or organosilicon compounds, which provide increased efficiency of drug binding [23]. There is also interest in the use of magnetic nanoparticles for hyperthermia [24], and interest in this direction consists in the heating efficiency enhancement through various modification methods, including the use of various stabilizing additives [25], the use of rare earth materials for partial replacement of cations, which leads to increased efficiency and a change in magnetic properties [26]. Moreover, among the variety of ferrite nanoparticles, one can distinguish nanostructures based on compounds of iron oxide with zinc oxide, the variation of the components of which makes it possible to obtain a spinel structure of the $ZnFe_2O_4$ type, which is one of the soft magnetic materials with high biocompatibility, non-toxicity, and also good conductive characteristics [27–29]. In this regard, great interest in this area of research is due to the search for a simple and cheap way to obtain such structures that have all the properties of zinc and iron oxides, as well as their characterization to expand the fundamental understanding of the properties of these nanostructures [30,31].

The aim of this study is to explore the prospects for using composite nanoparticles based on Fe_3O_4/ZnO compounds as a basis for hyperthermic tests. The main emphasis in the work is on a detailed study of phase transformations and changes in ultrafine magnetic parameters in Fe_3O_4/ZnO nanoparticles obtained by a two-stage production method. The proposed method for obtaining Fe_3O_4/ZnO nanoparticles is one of the simplest and cheapest methods for obtaining nanostructures, which opens up the possibility of production of nanostructures on an industrial scale, which further allows expansion of the potential for the use of such nanostructures. In turn, a detailed study of the relationship between the conditions of production, structural features and ultrafine parameters of the magnetic field will make it possible to determine the optimal conditions for obtaining nanostructures for their practical application.

2. Materials and methods

The synthesis of Fe_3O_4/ZnO nanoparticles was carried out in three main stages. The first stage consisted of chemical precipitation of Fe_3O_4 nanoparticles by dissolving 3.25 g of $FeCl_3 \cdot 6H_2O$ in 100 ml of water with the addition of 5 ml of Na_2SO_3 (5 %), followed by mixing the resulting mixture with 20 ml of ammonia and heating for 30 minutes at a temperature of 70 °C. All experiments were carried out in an argon box. The addition of citric acid to the resulting mixture allowed the precipitate to be stabilized, followed by evaporation at a temperature of 90 °C for 90 minutes and washing in distilled water to remove reaction products in the form of chlorides.

The second stage of the synthesis consisted of mechanochemical mixing of the resulting Fe_3O_4 nanoparticles with zinc oxide (ZnO) using a PULVERISETTE 6 classic line planetary mill (Fritsch, Berlin, Germany). Grinding was carried out in an 80 ml beaker made of tungsten carbide using grinding balls with a diameter of 10 mm. The ratio of the grinding volume of the initial components from the grinding media was 1:3. The ratio of the Fe_3O_4 and ZnO components was chosen to be 1:1. Grinding was carried out at a speed of 400 rpm for 30 minutes, followed by removing the ground mixture from the glass.

The third stage of the synthesis consisted of a thermal isochronous annealing process in the temperature range from 100 to 1000 °C in increments of 100 °C for 5 hours. The heating rate was 10 °C/min, the cooling time of the samples after sintering varied from several hours to one day. The choice of such a wide temperature range is due to the possibility of studying the processes of phase transformations when changing the annealing temperature, as well as assessing the influence of annealing conditions on the properties of the resulting nanostructures. As a result of experimental work on thermal annealing, a series of samples was obtained, which was subsequently comprehensively studied to determine the effect of annealing temperature on the processes of structural changes, as well as to establish the relationship between phase transformations and the properties of nanoparticles.

The study of phase transformations in the structure of synthesized Fe_3O_4/ZnO nanoparticles depending on the temperature of isochronous thermal annealing was carried out using the method of X-ray phase analysis, through a comparative analysis of the observed changes in X-ray diffraction patterns. Diffraction patterns were obtained on MiniFlex600 powder diffractometer (Rigaku, Japan). The diffraction patterns were recorded in the Bragg-Brentano geometry in the angular range $2\theta = 25–90°$, with a step of 0.03°.

Determination of the phase composition of the studied Fe_3O_4/ZnO nanoparticles depending on the annealing temperature was performed by comparing the observed X-ray diffraction patterns with the reference values of various phases of ferrites and iron oxides, which were taken from the PDF-2 (2016) database. The crystal lattice parameters were refined considering a priori information about the methods for producing Fe_3O_4/ZnO nanoparticles, as well as the associated structural distortions, as a result of mechanochemical synthesis and subsequent thermal annealing.

The morphological features of the synthesized Fe_3O_4/ZnO nanoparticles were studied using scanning electron microscopy and transmission electron microscopy. To implement these methods, microscopes JEOL 7500F (Jeol, Tokyo, Japan) and Jeol JEM-1400Plus (Jeol, Tokyo, Japan) were used. The elemental composition of the synthesized Fe_3O_4/ZnO nanoparticles was studied using the energy dispersive analysis method, implemented using a Hitachi TM3030 (Hitachi, Tokyo, Japan) microscope.

Phase transformations in Fe_3O_4/ZnO nanoparticles during thermal

annealing were also studied using the Mössbauer spectroscopy method on ^{57}Fe nuclei, which made it possible to obtain additional information about iron-containing phases. Mössbauer spectra were recorded on a Mössbauer spectrometer MS1104Em operating in the constant acceleration mode with a triangular change in the Doppler velocity of the source relative to the absorber. The ^{57}Co nuclei in the Rh matrix served as a source of resonant γ-quanta. The spectra were obtained at room temperature. The spectra were processed using the SpectrRelax program [32].

The study of the influence of the phase composition of Fe_3O_4/ZnO nanoparticles by various methods on the heating rate and the change in the specific absorption rate was carried out using an SPG-10AB-II variable frequency induction heating unit manufactured by Shuangping Power Supply Technologies Company Ltd., (Shanghai city, China).

Experimental conditions: current value 20 A, alternating magnetic field with an amplitude of 210 Oe and a frequency of 320 kHz. The flask with the test solution was heated using a copper spiral with a diameter of 6 cm, consisting of 4 turns. The magnetic field strength was calculated based on the geometry of the coil and the magnitude of the current. The flask with the test solution was placed inside a magnetic coil and isolated from the environment to prevent heat transfer and heat loss. The temperature of the solution was monitored using fiber optic thermometers placed in the liquid; these changes were read every 5 seconds. Aqueous solutions with nanoparticles dissolved in them with a volume of 10 mg/ml were used as model solutions.

The specific absorption rate (*SAR*), which characterizes the thermal conductivity properties of nanoparticles, was calculated according to formula (1) [33]:

$$SAR = \frac{M}{m_{\text{nanoparticles}}} C_{water} \frac{\Delta T}{\Delta t} \tag{1}$$

where M is the mass of the solution, $m_{\text{nanoparticles}}$ is the mass of nanoparticles, C_{water} is the specific heat capacity of the solution, $\Delta T/\Delta t$ is the slope of the temperature curve.

Due to the low concentration of nanoparticles, their heat capacity was not taken into account, and the specific heat of water was chosen as C_{water}.

The intrinsic loss power (*ILP*) value, which is expressed as a quadratic dependence on the magnetic field and a linear dependence on frequency, usually allows one to compare the heating efficiency in hyperthermic studies carried out with different samples or at different magnetic field strength parameters. To determine the value of ILP, expression (2) was used [34]:

$$ILP = SAR/H^2 f, \tag{2}$$

where H is the applied field strength, f is the frequency.

The M − H curves measurements were carried out using a vibrational magnetometer system (VSM, Liquid Helium Free High Field Measurement System "Cryogenic Ltd."). The measurements were carried out in a magnetic field H = ± 10 000 Oe, at room temperature.

To determine the efficiency of using synthesized nanoparticles as a basis for hyperthermic applications, considering their biocompatibility (in order to determine the absence of a negative impact on living organisms, in this case cellular structures), an MTT test was conducted. Mia PaCa 2 cell lines were used as the cell structure, and a solution (3-[4,5-dimethylthiazol-2yl]-2,5-diphenyltetrazolium bromide) was used as the MTT test. Measurements were performed at three different nanoparticle concentrations of 10, 50 and 100 μg. The test times were 24, 48, 72 and 168 hours. After each test time, the cell line survival was assessed.

3. Results and discussion

Fig. 1 illustrates the results of X-ray phase analysis of synthesized Fe_3O_4/ZnO nanoparticles depending on the temperature of thermal isochronous annealing in the range from 100 to 1000 °C with a step of 100 °C, reflecting the processes of phase transformations and structural ordering contingent upon the annealing temperature. The general appearance of the presented X-ray diffraction patterns when assessing changes in the shape and position of reflections indicates both the processes of phase transformations and the associated structural ordering with the thermal annealing temperature growth. Moreover, these processes of phase transformations have a pronounced temperature dependence, which indicates that these processes are associated primarily with thermal effects that arise during thermal heating of samples, and, as a consequence, changes in the magnitude of thermal vibrations in the structure. Also, analysis of the shape of diffraction lines depending on the annealing temperature indicates processes of change in the degree of structural ordering associated with thermal annealing of defects

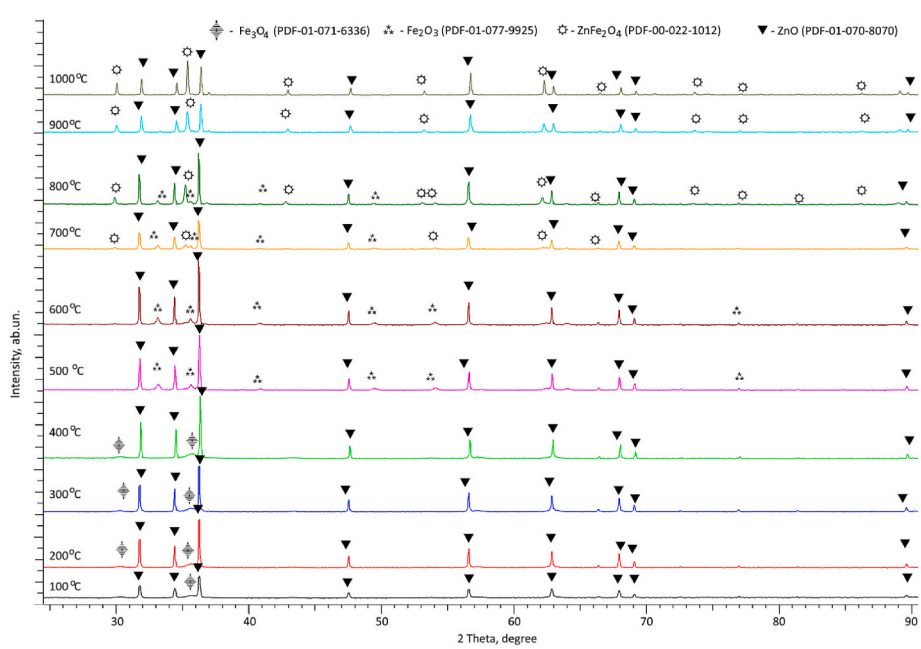

Fig. 1. Results of X-ray phase analysis of the studied Fe_3O_4/ZnO nanoparticles depending on the thermal annealing temperature.

arising during mechanochemical synthesis.

In the case of samples obtained at an annealing temperature of 100 °C, diffraction reflections characteristic of two phases were recorded in the diffraction pattern: the hexagonal phase of ZnO (PDF-01-070-8070) and the cubic phase of magnetite Fe_3O_4 (PDF-01-071-6336). At the same time, the dominant phase, according to the assessment of the weight contributions of diffraction reflections, is the ZnO phase, the content of which is more than 80 %. The low content of the magnetite phase is due to the low structural ordering degree associated with the chemical precipitation processes, alongside subsequent mechanochemical grinding. At the same time, it should be noted that the shapes of diffraction reflections for both phases have a pronounced asymmetry, indicating structural distortion and deformation of the crystal lattice associated with mechanochemical grinding. At low annealing temperatures, phase transformation processes are not initialized, and the main structural changes are associated with structural ordering, which has a clear dependence on the thermal annealing temperature.

An elevation in the annealing temperature from 200 °C to 400 °C also does not lead to an alteration in the phase composition, but only to an increase in the intensity of diffraction reflections characteristic of the Fe_3O_4 – magnetite phase, the contribution of which increases from 15 to 36 %. This change indicates processes of structural ordering, leading to an increase in the contribution of the Fe_3O_4 magnetite phase due to its stabilization, as well as a slight enlargement of crystallite sizes from 15 to 20 nm (estimated using the Scherrer equation).

At an annealing temperature of 500 °C, according to the analysis of X-ray diffraction patterns, a phase transformation process of the $Fe_3O_4 \rightarrow Fe_2O_3$ type is observed, which is also accompanied by a change in structure from cubic to rhombohedral. Similar processes are quite well known for iron oxide nanoparticles, characterizing phase transformations that lead not only to changes in structural features, but also to a restructuring of magnetic and conductive properties due to changes in the local environment of the atoms [35–37].

A growth in the annealing temperature from 500 °C to 600 °C leads to a change in the structural ordering degree, and is also typical for the enlargement of crystallite sizes, which is consistent with the data of [38], in which it was demonstrated that subsequent thermal annealing of samples of iron oxide nanoparticles during the transformation from $Fe_3O_4 \rightarrow Fe_2O_3$ is accompanied by an enlargement of grain sizes due to sintering processes.

At an annealing temperature of 700 °C, a second phase transformation occurs, associated with the formation of a spinel structure of $ZnFe_2O_4$ (PDF-00-022-1022) with a cubic type of crystal lattice, the formation of which is due to the processes of substitution of iron ions in the Fe_2O_3 structure by zinc ions with their subsequent transformation into a spinel structure. The formation of the $ZnFe_2O_4$ phase, according to several works [39,40], occurs at elevated annealing temperatures, and in some cases the formation of two-phase or three-phase structures with both magnetic and dielectric properties is possible.

A further annealing temperature growth from 700 to 900 °C results in complete transformation of the Fe_2O_3 – hematite phase into the $ZnFe_2O_4$ phase, with its dominance at annealing temperatures of 900–1000 °C.

Based on the analysis of the weight contributions of diffraction reflections for each established phase, depending on the temperature of thermal isochronous annealing, a phase diagram for Fe_3O_4/ZnO nanoparticles was constructed, which is presented in Fig. 2a.

Analyzing the data presented in Fig. 2a, we can distinguish three characteristic stages of changes in structural features in Fe_3O_4/ZnO nanoparticles depending on the thermal annealing temperature. The first stage is characteristic of the structural ordering of the Fe_3O_4 phase – magnetite at annealing temperatures from 100 to 400 °C, which leads to a rise in its contribution, and a change in the shape of diffraction reflections. The second stage is characteristic of phase transformation processes such as $Fe_3O_4 \rightarrow Fe_2O_3$ and subsequent structural ordering of the hematite phase, occurring at thermal annealing temperatures of 500–600 °C. The third stage is characterized by processes of phase transformations such as Fe_2O_3/ZnO → $ZnFe_2O_4$, followed by the displacement of the Fe_2O_3 phase and the dominance of the $ZnFe_2O_4$ phase in the composition of nanoparticles.

Thus, the general dynamics of phase transformation processes in Fe_3O_4/ZnO nanoparticles depending on the temperature of thermal isochronous annealing can be written in the following form: Fe_3O_4/ZnO → Fe_2O_3/ZnO → Fe_2O_3/ZnO/$ZnFe_2O_4$ → $ZnFe_2O_4$/ZnO. It should be noted that the established phase transformations Fe_3O_4/ZnO → Fe_2O_3/ZnO → Fe_2O_3/$ZnFe_2O_4$ → $ZnFe_2O_4$/ZnO in this work refer to the obtained ratio ZnO:Fe_3O_4 in equal parts 1:1. It should be noted that the established phase transformations of the Fe_3O_4/ZnO → Fe_2O_3/ZnO type, arising in the temperature range of 100–500 °C, are in good agreement with the results of phase transformations for $Fe_3O_4 \rightarrow Fe_2O_3$ nanoparticles obtained in Refs. [31,38]. It should also be noted that the established fact of the formation of the $ZnFe_2O_4$ phase occurs at a temperature above 600 °C is in good agreement with the results of work [7], which describes in detail the processes of the influence of heat treatment under various conditions.

Based on a full-profile analysis of the shape of diffraction reflections, the structural ordering degree (degree of crystallinity (K)) was determined, calculated based on determination of the ratio of the areas of diffraction reflections (S_{ref}) and background radiation characteristic of a disordered structure (S_{amorph}). For the calculation, formula (3) was used. The evaluation results are presented in Fig. 2b.

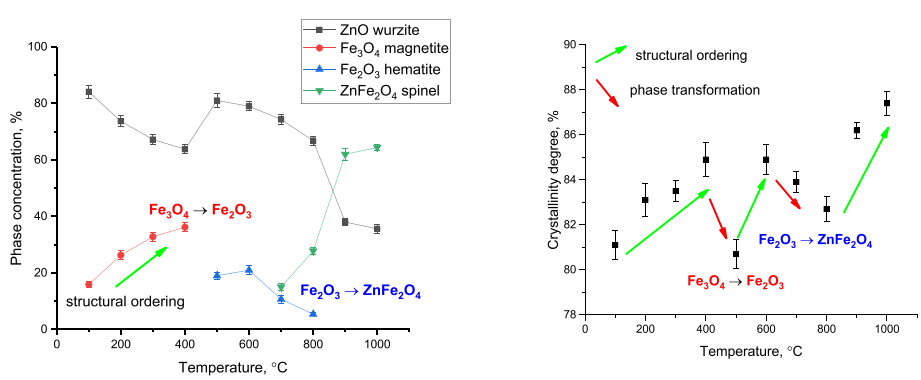

a) b)

Fig. 2. a) Phase diagram of Fe_3O_4/ZnO nanoparticles depending on the temperature of thermal isochronous annealing; b) Dependence of the change in the crystallinity degree of Fe_3O_4/ZnO nanoparticles with changes in the annealing temperature (arrows reflect the main processes of structural changes that have a direct effect on the change in the crystallinity degree).

$$K = \frac{S_{ref}}{S_{amorph} + S_{ref}} \times 100\ \%, \quad (3)$$

The general form of the presented dependence of the change in the degree of crystallinity on the temperature of thermal isochronous annealing is characterized by two types of structural changes associated with structural ordering and phase transformations leading to a change in the degree of crystallinity. With an increase in the thermal annealing temperature from 100 to 400 °C, an increase in the degree of crystallinity is observed, which is due to the processes of thermal annealing of defects, as well as the ordering of the crystal structure by filling vacancy positions due to an increase in thermal vibrations of the crystal lattice. At a temperature of 500 °C, phase transformations of the $Fe_3O_4 \rightarrow Fe_2O_3$ type occur, caused by deformation processes of the crystal lattice, leading to the crystallinity degree reduction due to phase rearrangement. A further elevation in the annealing temperature from 500 to 600 °C leads to ordering due to stabilization of the hematite phase. However, at a temperature of 700 °C, a decrease in the degree of crystallinity is associated with phase formation processes such as Fe_2O_3/ZnO → $ZnFe_2O_4$, as well as the displacement of the hematite phase, the presence of which at an annealing temperature of 800 °C leads to a decrease in the degree of structural ordering. In turn, the complete displacement of the hematite phase from nanoparticles through its transformation into the spinel phase of $ZnFe_2O_4$ at annealing temperatures of 900–1000 °C leads to a rise in structural ordering, and a decrease in amorphous inclusions in the structure of nanoparticles.

Based on the analysis of the obtained X-ray diffraction data, the parameters of the crystal lattice and its volume were estimated for each established phase depending on the temperature of thermal isochronous annealing. These assessments of structural parameters are demonstrated in Table 1.

The general trend of alterations in crystal lattice parameters depending on the annealing temperature indicates the processes of atomic ordering and compaction that occur with changes in thermal vibrations, alongside the filling of cation positions in octo and tetrahedral positions. These structural orderings are most pronounced during the formation of the $ZnFe_2O_4$ phase, an increase in the annealing temperature for which leads to a decrease in volume by more than 1 %, which indicates a reduction in deformation distortions in the structure. Also, the ordering of the $ZnFe_2O_4$ phase with increasing temperature may be due to a change in the ratio of elements, as well as the redistribution of Zn^{2+} and Fe^{3+} ions in interstices, due to the difference in the ionic radii of Zn^{2+} (0.74 Å) and Fe^{3+} (0.67 Å). The processes of phase transformations occurring at temperatures of 500 and 700 °C, meanwhile, result in distortion of the zinc oxide crystal lattice.

One of the important parameters for assessment of the nanoparticles' applicability for various practical applications is the size of their grains or crystallites, the change in which can be associated with both phase formation effects and thermal sintering processes leading to their sticking together to form large agglomerates. In most cases [41,42], thermal annealing at high temperatures results in the initialization of sintering or adhesion of nanoparticles associated with recrystallization processes. This change in the size of nanoparticles is usually associated with the fact that during high-temperature thermal annealing, oxidation processes occur when interacting with oxygen, which leads to the sticking together of particles with their subsequent transformation into larger agglomerates. In the case of composite nanostructures, the presence of different phases can also lead to the adhesion of nanoparticles into large agglomerates due to the difference in melting temperatures and phase transitions, the initialization of which can occur with increasing annealing temperature.

Fig. 3 presents the results of morphological studies in the form of images obtained using high-resolution transmission electron microscopy of Fe_3O_4/ZnO nanoparticles annealed at temperatures of 100, 500, 700 and 1000 °C. The choice of temperatures is determined by the characteristic processes of phase transformations in Fe_3O_4/ZnO nanoparticles associated with the transformation of magnetite into hematite, as well as the formation of the spinel phase of $ZnFe_2O_4$.

Table 1
Data on the crystal lattice parameters and volume for Fe_3O_4/ZnO nanoparticles.

Temperature, °C	Lattice parameter and volume			
	ZnO – Wurtzite	Fe_3O_4 – Magnetite	Fe_2O_3 – Hematite	$ZnFe_2O_4$ –Spinel
100	a = 3.2508 ± 0.0013 Å, c = 5.2069 ± 0.0012 Å, V = 47.68 Å^3	a = 8.3532 ± 0.0016 Å, V = 582.84 Å^3	–	–
200	a = 3.2476 ± 0.0012 Å, c = 5.2049 ± 0.0017 Å, V = 47.54 Å^3	a = 8.3465 ± 0.0014 Å, V = 581.45 Å^3	–	–
300	a = 3.2483 ± 0.0017 Å, c = 5.2019 ± 0.0012 Å, V = 47.53 Å^3	a = 8.3432 ± 0.0017 Å, V = 580.75 Å^3	–	–
400	a = 3.2399 ± 0.0013 Å, c = 5.1957 ± 0.0017 Å, V = 47.23 Å^3	a = 8.3365 ± 0.0013 Å, V = 579.36 Å^3	–	–
500	a = 3.2482 ± 0.0017 Å, c = 5.2039 ± 0.0015 Å, V = 47.55 Å^3	–	a = 5.0297 ± 0.0015 Å, c = 13.7486 ± 0.0013 Å, V = 301.21 Å^3	–
600	a = 3.2507 ± 0.0013 Å, c = 5.3081 ± 0.0015 Å, V = 47.66 Å^3	–	a = 5.0337 ± 0.0015 Å, c = 13.7565 ± 0.0012 Å, V = 301.86 Å^3	–
700	a = 3.2513 ± 0.0012 Å, c = 5.2071 ± 0.0014 Å, V = 47.67 Å^3	–	a = 5.0386 ± 0.0015 Å, c = 13.7376 ± 0.0013 Å, V = 302.04 Å^3	a = 8.4494 ± 0.0016 Å, V = 603.22 Å^3
800	a = 3.2518 ± 0.0012 Å, c = 5.2092 ± 0.0015 Å, V = 47.70 Å^3	–	a = 5.0427 ± 0.0014 Å, c = 13.7486 ± 0.0012 Å, V = 302.77 Å^3	a = 8.4477 ± 0.0015 Å V = 602.86 Å^3
900	a = 3.2359 ± 0.0016 Å; c = 5.1884 ± 0.0012 Å, V = 47.05 Å^3	–	–	a = 8.4139 ± 0.0013 Å; V = 595.54 Å^3
1000	a = 3.2347 ± 0.0015 Å; c = 5.1822 ± 0.0017 Å; V = 46.96 Å^3	–	–	a = 8.4101 ± 0.0012 Å, V = 594.83 Å^3

As is evident from the presented images, in the case of thermal annealing at 100 °C, the presence of two types of particles with different shapes is observed. Elemental analysis suggests that the much larger hexagonal particles are zinc oxide, which is characterized by a hexagonal or feather-shaped particle shape (see data in Fig. 1 in Supplementary material). At the same time, the sizes of ZnO particles differ significantly from the sizes of particles having a spherical shape, characteristic of Fe_3O_4 nanoparticles.

An elevation in the annealing temperature to 500 °C, resulting in phase transformations such as $Fe_3O_4 \rightarrow Fe_2O_3$, is accompanied by a slight enlargement of particles, with the formation of larger particles characteristic of hematite, which is in good agreement with the data from the analysis of the structural features of the synthesized nanoparticles. At the same time, the formation of $ZnFe_2O_4$ nanoparticles leads to further coarsening of the particles, as well as isotropy and

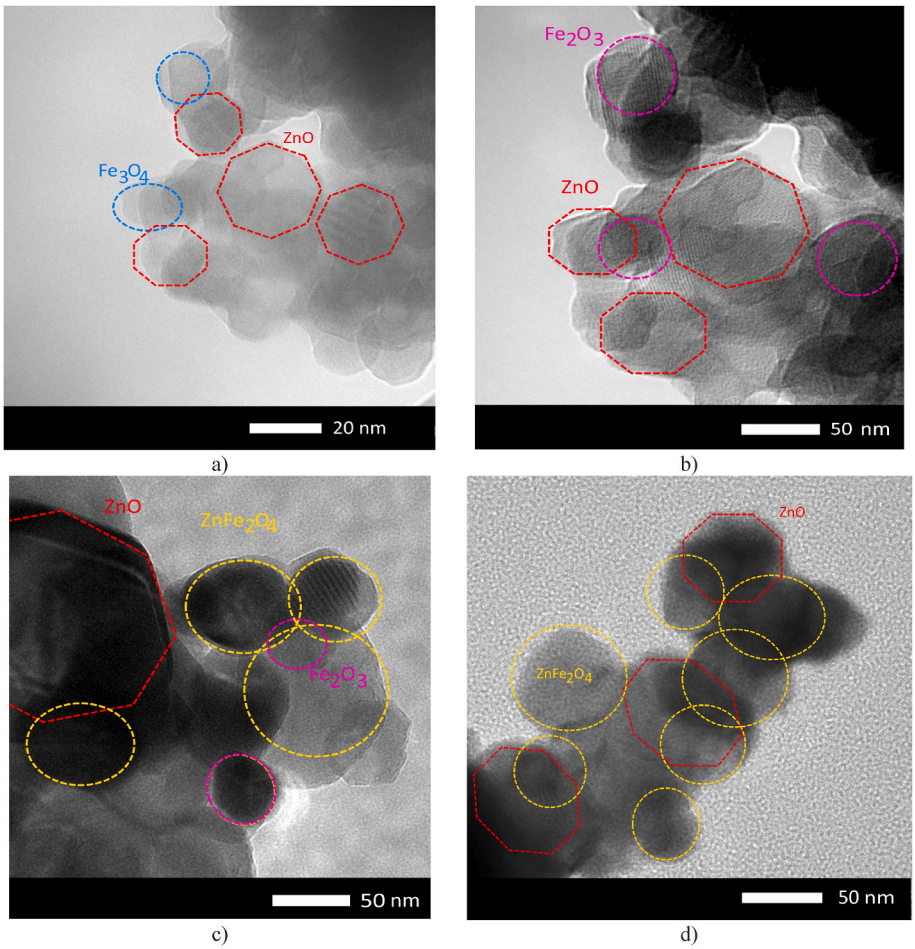

Fig. 3. TEM images of synthesized Fe_3O_4/ZnO nanoparticles at different thermal annealing temperatures, reflecting changes in the size and shape of nanoparticles: a) 100°C; b) 500°C; c) 700°C d) 1000°C.

uniformity of both the shape and size of the particles, which was not observed at lower annealing temperatures (see data in Fig. 2 in Supplementary material).

In the case of the initial Fe_3O_4 nanoparticles obtained by chemical precipitation in the initial state before thermal annealing the phase composition is represented by the magnetite $Fe_{3-\gamma}O_4$ structure with a highly disordered structure. At the same time, in the structure of nanoparticles before thermal annealing, it is not possible to establish the exact weight fraction of γ-Fe_2O_3 due to the highly disordered structure, alongside the difference in stoichiometry. Moreover, the change in the oxidation state in the structure of nanoparticles depending on annealing has a clearly expressed dependence on the annealing temperature, an increase in which results in phase transformations caused by transformations of the Fe_3O_4/ZnO → Fe_2O_3/ZnO → Fe_2O_3/$ZnFe_2O_4$ → $ZnFe_2O_4$/ZnO type. A detailed change in the oxidation state was studied using the Mössbauer spectroscopy method.

Figs. 4 and 5 demonstrate the Mössbauer spectra of the studied Fe_3O_4/ZnO nanoparticles. As is evident, the spectra of nanoparticles, unannealed and annealed at temperatures of $t_{ann} \leq 400$ °C (Fig. 4), are mainly a Zeeman sextet with signs of relaxation behavior of nanoparticles. Based on data obtained by X-ray diffractometry and electron microscopy, it can be assumed that these iron-containing nanoparticles correspond to Fe_3O_4 oxide.

Double iron (II,III) oxide Fe_3O_4 in nanoparticles, which can exhibit relaxation behavior, can be represented as non-stoichiometric magnetite $Fe_{3-\gamma}O_4$. In accordance with this, the spectrum of double iron oxide was generally described within the framework of the multilevel superparamagnetic relaxation model [43] by three partial relaxation spectra corresponding to Fe atoms in three different structural and valence states: trivalent Fe^{3+} ions in the tetrahedral (A) and octahedral (B) positions – Fe_A^{3+} and Fe_B^{3+}, and $Fe^{2.5+}$ ions in the octahedral position – $Fe_B^{2.5+}$ of the magnetite structure. A detailed description of the model of the spectrum of double iron oxide nanoparticles, which considers both possible superparamagnetic relaxation and fast electron exchange between neighboring Fe_B^{2+} and Fe_B^{3+} atoms in the octahedral position [44, 45], is presented in our previously published works [46,47]. This model makes it possible to determine not only the hyperfine parameters of the spectrum of double iron oxide (II,III) Fe_3O_4, but also the number of vacancies in the octahedral position of Fe ($0 \leq \gamma \leq 1/3$) atoms per formula unit $Fe_{3-\gamma}O_4$ (degree of nonstoichiometry of magnetite $Fe_{3-\gamma}O_4$), a parameter of the multilevel superparamagnetic relaxation model (α), equal to the ratio of the magnetic anisotropy energy E_{ma} to the thermal energy k_BT, the magnetic anisotropy coefficient at room temperature (K_{eff}), as well as the size of the magnetic ordering region (d).

Along with the partial spectra of double iron oxide (II,III) Fe_3O_4, in the center of the Mössbauer spectra of unannealed and annealed Fe_3O_4/ZnO nanoparticles at 100–400^{0}C, a low-intensity (<3 %) quadrupole doublet is observed (Fig. 4). Ultrafine parameters of the quadrupole doublet: isomer shift δ ~0.11–0.14 mm/s and quadrupole shift ε ~0.19–0.23 mm/s, correspond to Fe^{3+} atoms in a paramagnetic state with a tetrahedral oxygen environment, presumably dissolved or incorporated into the lattice of zinc oxide ZnO (ZnO:Fe) [48–50] during the mechanochemical synthesis.

At temperatures above 400^{0}C, a dramatic change in the appearance of the Mössbauer spectra is observed - a new Zeeman sextet and a second

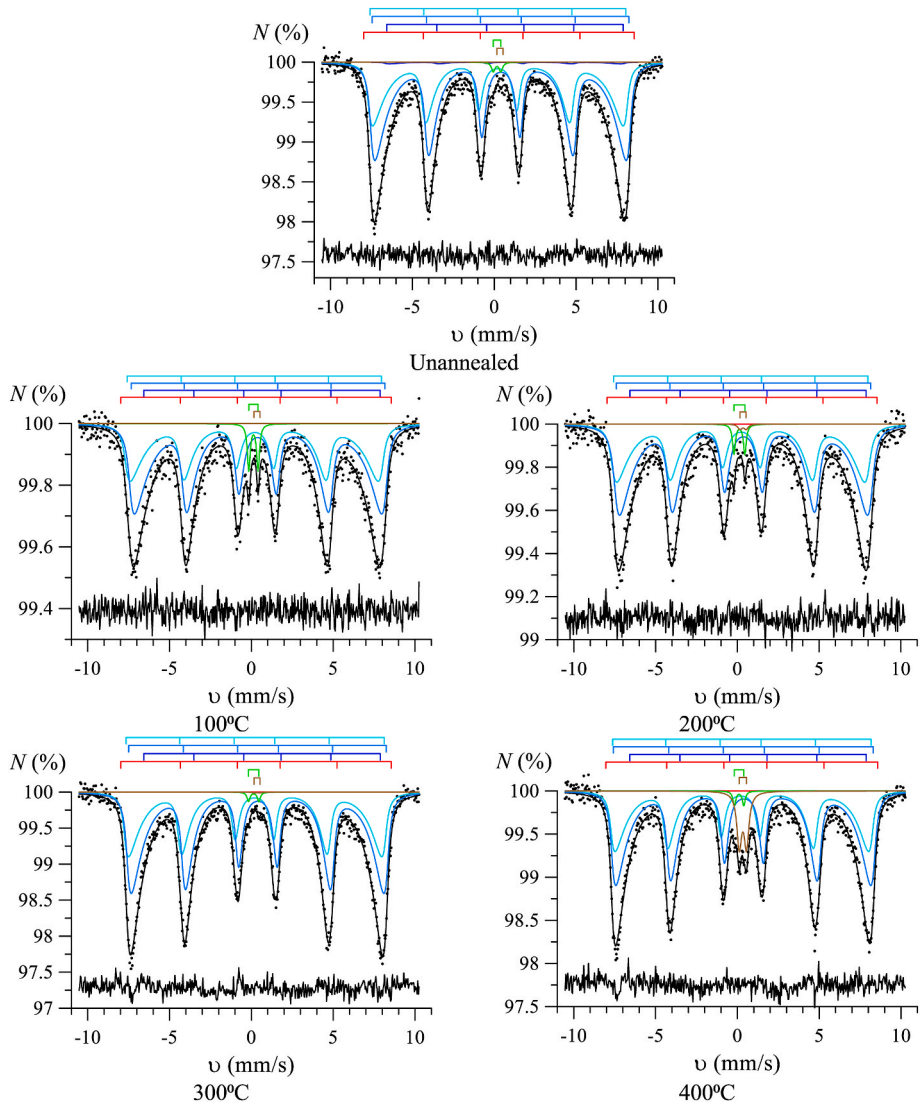

Fig. 4. Results of interpretation of the Mössbauer spectra of unannealed and annealed Fe_3O_4/ZnO nanoparticles at 100, 200, 300 and 400 °C.

quadrupole doublet appear, the contribution of which increases with increasing annealing temperature (Fig. 5). According to X-ray diffraction and electron microscopy data, the sextet corresponds to hematite α-Fe_2O_3, and the doublet corresponds to the spinel phase of $ZnFe_2O_4$, which is in a paramagnetic state at room temperature [51,52].

Thus, in the general case, the interpretation of the spectra of Fe_3O_4/ZnO nanoparticles was carried out using a model consisting of three interconnected relaxation partial spectra of double iron oxide (II,III) Fe_3O_4 (corresponding to the Fe_A^{3+}, Fe_B^{3+} and $Fe_B^{2.5+}$ atoms), to which an independent Zeeman sextet corresponding to hematite and two quadrupole doublets corresponding to ZnO oxide with impurity atoms Fe (ZnO:Fe) and $ZnFe_2O_4$ (Figs. 4 and 5) were added. The figures above each spectrum show color bar diagrams of the positions of the resonance lines of partial spectra (subspectra), corresponding to different phases ($Fe_{3-\gamma}O_4$ – blue, α-Fe_2O_3 – red, ZnO:Fe – brown, $ZnFe_2O_4$ – green). As is evident, all experimental spectra are well described within the framework of the model used: normalized chi-square values range from 0.84 to 1.29.

Fig. 6a illustrates the relative intensities of partial spectra corresponding to different states of Fe atoms in Fe_3O_4/ZnO nanoparticles, depending on the annealing temperature t_{ann}. Analysis of the data obtained reveals that the intensity of the partial spectrum of $Fe_B^{2.5+}$ ($Fe_{3-\gamma}O_4$) atoms is practically zero. This means that double iron oxide (II,III) Fe_3O_4 in unannealed and annealed nanoparticles is a non-stoichiometric magnetite with a maximum degree of non-stoichiometry $\gamma \cong 1/3$, that is, almost pure maghemite γ-Fe_2O_3.

Above the annealing temperature of 400 °C, the relative intensity of the partial spectra corresponding to the Fe_A^{3+} and Fe_B^{3+} states of Fe atoms in $Fe_{3-\gamma}O_4$ sharply decreases from 97 to 99 % to 7.2 ± 0.2 %, and the intensity of the spectrum of Fe^{3+} atoms in α-Fe_2O_3 hematite rises sharply to 87.7 ± 0.3 %. At the same time, the spectrum reveals a partial spectrum of Fe atoms in the spinel phase of $ZnFe_2O_4$ with a relative intensity of 5.1 ± 0.2 %. With a further increase in the annealing temperature above 600 °C, a decrease in the intensity of the α-Fe_2O_3 spectrum to 20.5 ± 0.8 % at a temperature of 1000 °C is observed, accompanied by a corresponding increase in the intensity of the $ZnFe_2O_4$ spectrum to 79.5 ± 0.8 %.

To compare the results of X-ray and Mössbauer phase analyses, Fig. 6b demonstrates the relative contributions to the Mössbauer spectrum (MS) and X-ray diffraction pattern (XRD) of iron-containing phases in Fe_3O_4/ZnO nanoparticles as a function of annealing temperature. Note that the main features of the change in the relative contributions to the Mössbauer spectrum and the X-ray diffraction pattern with increasing annealing temperature are quite well consistent with each other.

As a result of the model interpretation of Mössbauer spectra in the

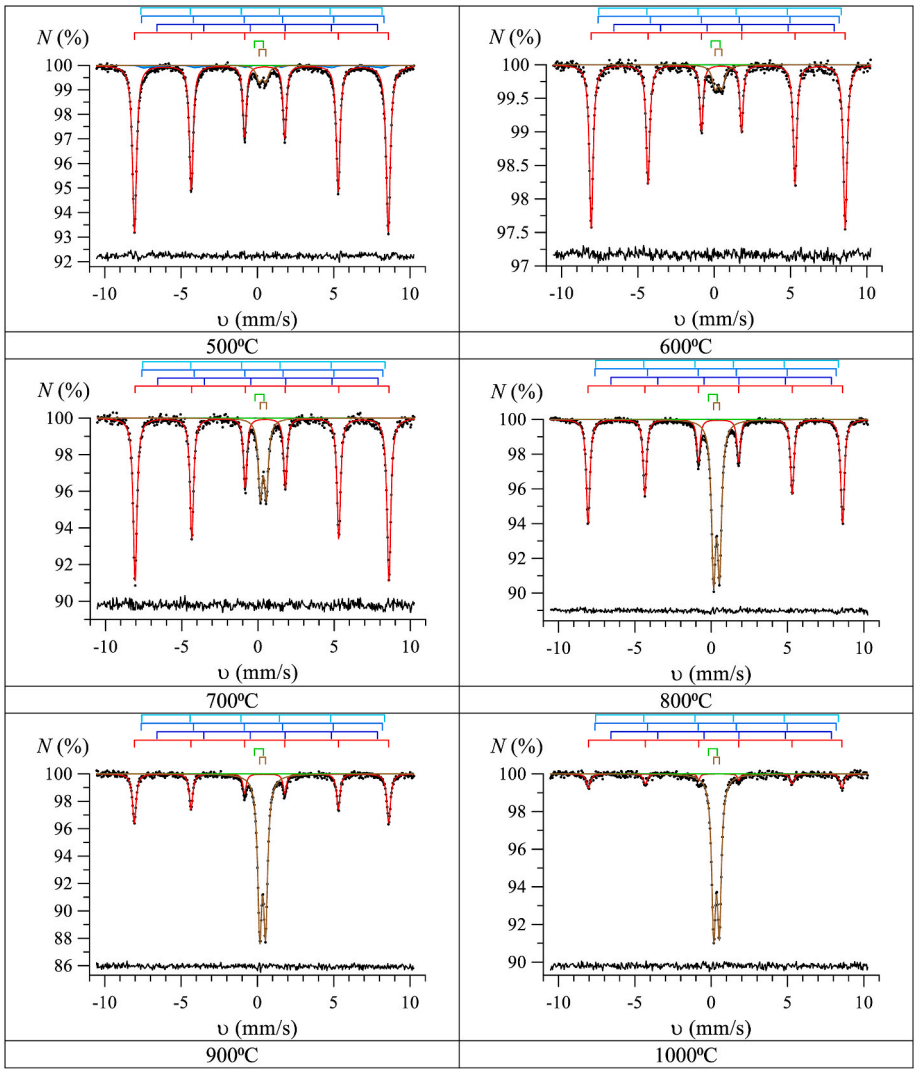

Fig. 5. Results of interpretation of the Mössbauer spectra of unannealed and annealed Fe_3O_4/ZnO nanoparticles at 500, 600, 700, 800, 900 and 1000 °C.

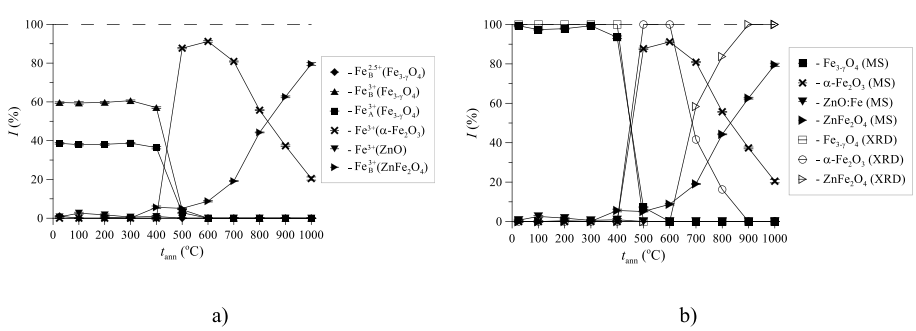

a) b)

Fig. 6. a) Relative intensities of partial spectra corresponding to different states of Fe atoms in Fe_3O_4/ZnO nanoparticles, depending on the annealing temperature t_{ann}; b) Relative contributions to the Mössbauer spectrum (MS) and X-ray diffraction pattern (XRD) of iron-containing phases in Fe_3O_4/ZnO nanoparticles depending on the annealing temperature t_{ann}.

range of annealing temperatures at which double iron oxide (II,III) Fe_3O_4 is determined in the form of maghemite γ-Fe_2O_3 the values of the multilevel superparamagnetic relaxation model parameter α and the magnetic anisotropy energy $E_{ma} = \alpha k_B T$ uniquely associated with it at a given temperature (295 K), which increase monotonically with annealing temperature growth (see Fig. 3a in Supplementary material), were obtained.

Since in our case the double iron oxide (II,III) Fe_3O_4 in unannealed and annealed Fe_3O_4/ZnO nanoparticles is practically pure maghemite γ-Fe_2O_3, the effective magnetic anisotropy coefficient K_{eff} was taken equal to (4.95 ± 0.75) 10^3 J/m3 [46,47]. Using this value of the coefficient K_{eff} and the magnetic anisotropy energy E_{ma}, the average sizes of the magnetic ordering regions $d = \left(\frac{6E_{ma}}{\pi K_{eff}}\right)^{\frac{1}{3}}$ of Fe atoms in double iron oxide were calculated, presented in Fig. 3b in Supplementary material. It

is evident that as the annealing temperature rises, the average sizes of these regions increase slightly from 20.5 ± 0.2 to 21.6 ± 0.3 nm due to their structural and magnetic ordering. Note that the average sizes of regions of magnetic ordering are consistent with data on the sizes of regions of structural ordering and particle sizes obtained using X-ray diffractometry and transmission electron microscopy.

As a result of the model decoding of the Mössbauer spectra of Fe_3O_4/ZnO nanoparticles subjected to thermal annealing, the values of ultrafine parameters of the partial spectra (ultrafine magnetic fields H_n, spectral shifts δ and quadrupole shifts of resonance lines ε), which made it possible to identify the partial spectra and analyze their dependence on the annealing temperature, were obtained.

Fig. 3c and d in Supplementary material, which present the ultrafine parameters of the partial spectra of nonstoichiometric magnetite $Fe_{3-\gamma}O_4$, show that the spectral shifts δ for ferric iron ions vary in the ranges of 0.20–0.23 mm/s and 0.37–0.40 mm/s (Fig. 10c), which is typical for tetrahedral (A) and octahedral (B) oxygen environments in the $Fe_{3-\gamma}O_4$ structure, respectively.

Ultrafine magnetic fields H_n on ^{57}Fe nuclei for ferric iron ions in tetrahedral and octahedral positions are quite close ($\left|H_n^B - H_n^A\right| \leq 4$ kOe) and, in contrast to other ultrafine parameters for these ions, at $t_{ann} \leq 400°C$ they increase markedly with growing annealing temperature (Fig. 10d). Since the annealing temperature growth, as shown above, does not change the limiting degree of nonstoichiometry of magnetite, such an increase in ultrafine magnetic fields indicates an improvement in the structure, as evidenced by a decrease in the unit cell parameter (see Table 1). As for the quadrupole shifts, their values turned out to be close to zero ($|\varepsilon| \leq 0.04$ mm/s), which is typical for the partial spectra of nonstoichiometric magnetite $Fe_{3-\gamma}O_4$ [53,54].

The obtained values of the hyperfine parameters of the second quadrupole doublet, shift δ ~0.34 mm/s and quadrupole displacement ε ~0.20 mm/s, correspond to Fe^{3+} atoms in the octahedral position of the $ZnFe_2O_4$ spinel structure (see, for example, [51,52]).

The dependences of the hyperfine parameters of the partial spectrum of hematite α-Fe_2O_3 in Fe_3O_4/ZnO nanoparticles on the annealing temperature are presented in Fig. 4 in Supplementary material. It can be seen that the spectrum shift remains virtually unchanged (δ ~ 0.373 mm/s), and the hyperfine magnetic field H_n and the quadrupole shift ε of the hyperfine structure components increase slightly with increasing annealing temperature up to 900 °C, approaching the values corresponding to massive hematite [55,56]. Thus, it can be concluded that as the annealing temperature is increased, the crystal and magnetic structure of hematite is improved. However, at an annealing temperature of 1000 °C, the hyperfine magnetic field decreases to ~515 kOe, and the quadrupole shift to – 0.109 mm/s, which may be due to the introduction of Zn atoms into the hematite structure, leading to disruption of Fe–O–Fe exchange bonds.

Fig. 7a demonstrates the results of measurements of M − H curves of the studied nanoparticles depending on their annealing temperature, which affects the change in phase composition, and as a consequence, the grain sizes and their shape. Fig. 7b reveals the M_S values determined from the M − H curves shown in Fig. 7a, alongside the dominant phase in the nanoparticles and their shape, since these parameters are among the most important parameters affecting magnetic properties. The observed alterations in the M − H curves, expressed in the presence of a small hysteresis in this case, can be explained by a number of factors, the key one of which is the size and shape of the grains, alongside the variation in the structural ordering degree associated with the phase formation processes during thermal annealing. According to the data obtained, the crystal structure ordering at an annealing temperature of 100–400°C results in the MS value growth from 81.5 emu/g to 94.3 emu/g, while the phase transition of the $Fe_3O_4 \rightarrow Fe_2O_3$ type leads to an insignificant increase in the M_S value to 97.1–98.2 emu/g. The formation of the $ZnFe_2O_4$ phase in the structure of nanoparticles with its subsequent doping results in the M_S value reduction to 74.4–77.9 emu/g. Such changes in this case may be due to the fact that spherical magnetic particles have higher values of saturation magnetization, the changes in which are due to the redistribution of cations in the structure. The compaction of grains (increase in their growth during thermal annealing) leads to the magnetic domains (crystallites) being in closer contact with each other, and according to X-ray phase analysis data, with an increase in the annealing temperature, structural ordering of the magnetic phase in the nanoparticles is observed. In this case, the compaction of particles leads to the provision of magnetic bonding of surface ions, which in turn allows for an increase in saturation magnetization. Phase transformations from $Fe_3O_4 \rightarrow Fe_2O_3$ to $ZnFe_2O_4$ lead to a change in the shape of particles, which in turn affects the reduction of the MS value, which is associated with both phase changes and observed structural effects. It should be noted that the observed M_S values for $ZnFe_2O_4$ are in good agreement with the results of a number of studies [57,58] obtained by the sol-gel method.

Thus, the analysis of the data obtained showed the connection between changes in the phase composition of nanoparticles and their sizes, caused by phase transformations under the influence of temperature and magnetic properties, both at the macro level (when measuring M − H curves) and during determination of hyperfine parameters (using the method of analyzing Mössbauer spectra).

Determination of biocompatibility of the studied nanoparticles, synthesized using the mechanosynthesis method and subsequent thermal annealing, was carried out using the MTT test at various

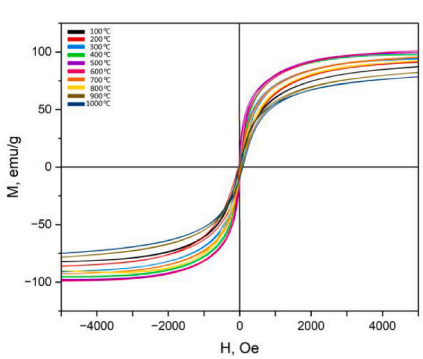

a)

Temperature of annealing, °C	M_S, emu/g	Dominant magnetic phase	Grain shape
100	81.5±1.3	Fe_3O_4	Finely dispersed fraction of spherical grains
200	85.2±1.1	Fe_3O_4	
300	90.4±2.1	Fe_3O_4	
400	94.3 ±1.9	Fe_3O_4	Enlargement of spherical grains
500	97.1±2.4	Fe_2O_3	
600	98.2±1.6	Fe_2O_3	mixture of elongated grains of $ZnFe_2O_4$ and spherical grains of Fe_2O_3
700	92.3±1.3	Fe_2O_3/$ZnFe_2O_4$	
800	89.8±1.5	$ZnFe_2O_4$	
900	77.9±1.6	$ZnFe_2O_4$	Small, uniformly sized, diamond-shaped particles
1000	74.4±1.2	$ZnFe_2O_4$	

b)

Fig. 7. a) Results of M − H curves measurements for the studied nanoparticles; b) Results of calculations of the M_S value.

concentrations of nanoparticles and test time intervals (from 24 to 168 hours). The results of the MTT tests for the studied nanoparticles are shown in Fig. 8. The general form of the presented data on the efficiency of cell survival depending on the concentration and time of testing has several dependencies. The first of the observed dependencies is associated with the concentration of nanoparticles, according to which an increase in the concentration of nanoparticles from 10 to 100 μg, in the case of structurally disordered particles (obtained at an annealing temperature of 100–500 °C) leads to a decrease in cell survival from 99 – 100 % to 97 %. At the same time, for nanoparticles in which the Fe_2O_3 and $ZnFe_2O_4$ phases dominate, the efficiency of cell survival after 24 hours remains unchanged. A similar situation is observed after 48 hours of testing, with a difference not only in the efficiency of cell survival (a decrease to 96–97 %), but also the manifestation of the effect of survival reduction at a nanoparticle concentration of 50 μg (the observed decrease is about 1–2 %). After 72 hours of testing, the effect of survival reduction (up to 1 %) is observed for nanoparticle concentrations of 10 μg, and with an increase in the concentration of nanoparticles, the maximum reduction is about 3 % for a concentration of 50 μg and about 5 % for a concentration of 100 μg. The observed reduction in this case can be explained not only by the effect of nanoparticles on cells, but also by corrosion products that arise as a result of prolonged exposure to the medium during the MTT test, which results in corrosion of the nanoparticles (see Data in Ref. [19]). More pronounced effects of the influence of long-term presence of nanoparticles in interaction with cell lines are manifested after 168 hours of testing, after which for nanoparticles obtained at annealing temperatures of 100–500 °C the survival rate is about 85–89 %, while for particles in which the $ZnFe_2O_4$ phase dominates the survival rate is about 95–96 %.

Thus, by analyzing the data obtained, it can be concluded that these nanostructures have good biocompatibility and do not have a negative impact on cellular structures.

As a rule, the use of ferrite nanoparticles as a basis for hyperthermic studies is primarily due to the possibility of local heating of nanoparticles when exposed to an alternating magnetic field, which leads to the release of a large amount of heat in a short period of time, which in turn causes apoptosis of cancer cells. At the same time, the unique magnetic characteristics, as well as the heat-conducting properties of ferrites, combined with their biocompatibility and non-toxicity, make them one of the most promising types of nanoparticles in their use as a basis for hyperthermic applications. Moreover, in the case of zinc ferrite, the spinel type of structure implies the fact that non-magnetic Zn^{2+} cations fill the sites of the A sublattice, which leads to the appearance of the effect of paramagnetism at room temperature, the use of which allows us to expand the possibilities of using ferrite nanoparticles as a basis for hyperthermal research.

Fig. 9a reveals the measurement results of the temperature dependences of heating of Fe_3O_4/ZnO nanoparticles.

As can be seen from the presented dependences of the change in the heating temperature of an aqueous solution (*T*) when exposed to an alternating magnetic field, the heating of the solution occurs with a different trend, which has a pronounced dependence on the type of nanoparticles, in particular, their phase composition. The change in the *T(t)* dependences for different nanoparticles indicates different types of heat transfer, as well as heat release processes when exposed to nanoparticles. In this case, as is evident from the data presented, an increase in heating time (*t*) in the case of nanoparticle samples containing inclusions in the form of particles of magnetite or hematite leads to a change in the trends in temperature heating, which may be due to both the effects of magnetic disorder and the presence of structurally disordered or amorphous inclusions.

Based on the presented *T(t)* dependences, the heating rates of the aqueous solution were calculated, reflecting the change in the temperature of the solution when nanoparticles are exposed to an alternating magnetic field over a certain time. The threshold value for calculations was T = 42.5 °C, a characteristic temperature for the treatment of cancer tumors using thermotherapy methods. The evaluation results are presented in Fig. 9b.

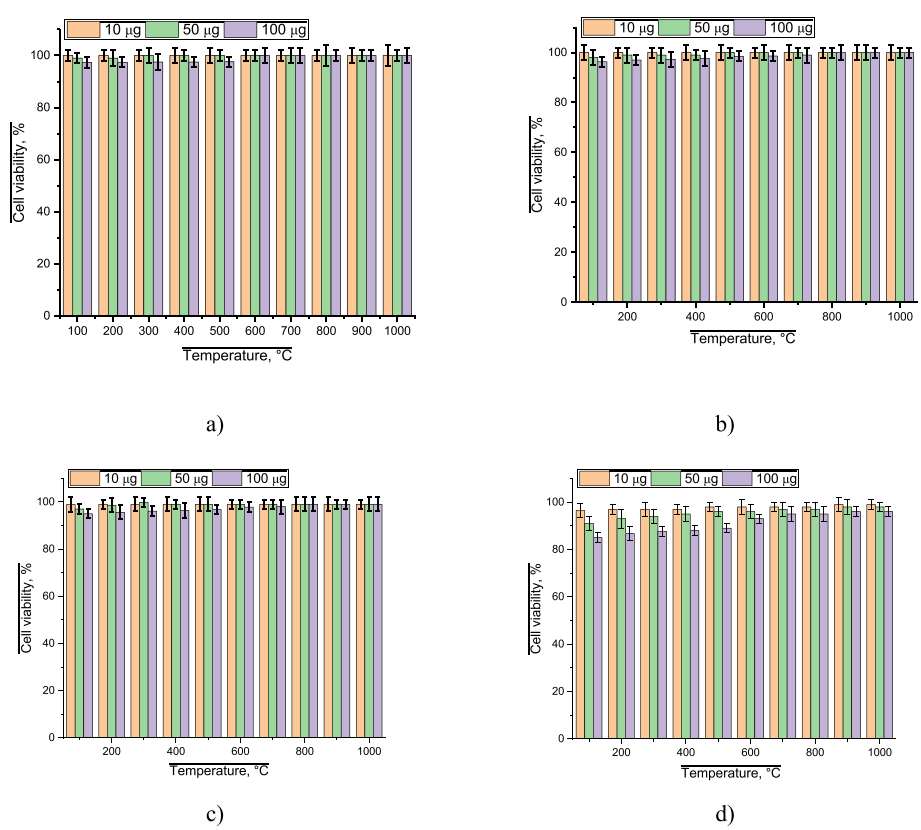

Fig. 8. Results of the MTT test of the studied nanoparticles depending on the test time: a) 24 hours; b) 48 hours; c) 72 hours; d) 168 hours.

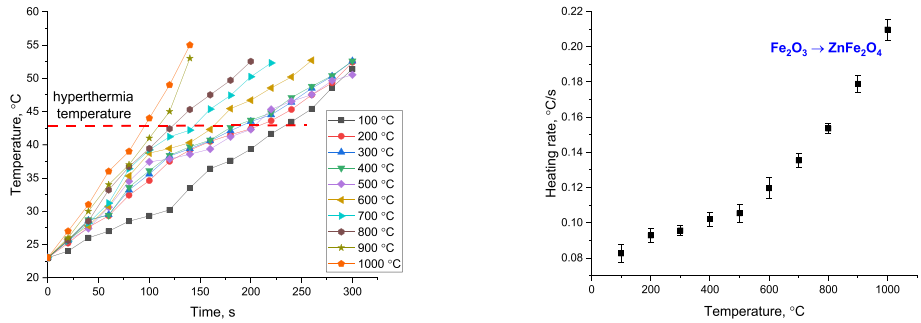

a) b)

Fig. 9. a) Results of measuring the dependence of the heating temperature of Fe_3O_4/ZnO nanoparticles on time (the dotted red line indicates a temperature of 42.5 °C, characteristic of hyperthermic tests); b) Results of the aqueous solution heating rate assessment.

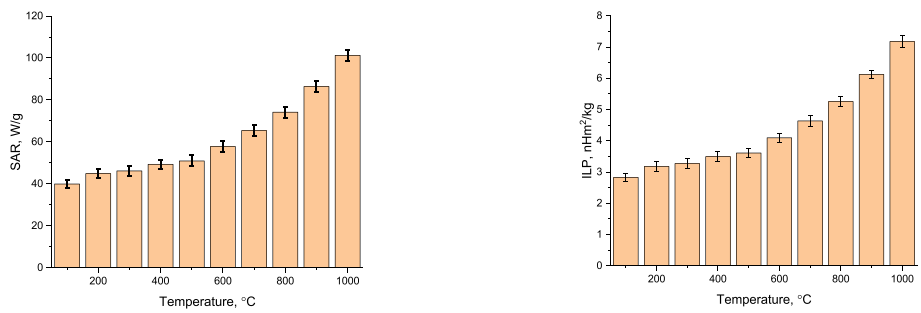

a) b)

Fig. 10. a) Results of the SAR value assessment depending on the annealing temperature, which is used to initiate phase and structural changes in Fe_3O_4/ZnO nanoparticles; b) Results of ILP value change assessment depending on the annealing temperature, which is used to initiate phase and structural changes in Fe_3O_4/ZnO nanoparticles.

As is evident from the data presented, a change in the synthesis conditions of nanoparticles, and therefore, a change in the phase composition, as well as the structural ordering degree, results in heating rate growth, the change in which may be due to alterations caused by improved heat transfer of nanoparticles, as well as variations in magnetic properties and the magnetic ordering degree. In the case of increasing the thermal annealing temperature in the temperature range 100–400 °C, a small change in the heating rate is observed, since the main processes at this stage are associated with structural ordering, as well as an increase in the ordering of the magnetite phase, which leads to an alteration in the value of magnetic anisotropy caused by distortion of the hyperfine parameters of the magnetic field, as well as the filling of A and B sublattices with vacancy defects or zinc atoms. Phase transformations such as $Fe_3O_4 \rightarrow Fe_2O_3$, occurring at annealing temperatures above 500 °C, result in the heating rate growth, which may be due to the effects of changes in magnetic characteristics, alongside structural ordering, leading to compaction of nanoparticles. In this case, in addition to the effects associated with magnetic ordering, leading to lower losses of thermal power due to dissipation when exposed to an external magnetic field.

During the transition of nanoparticles to the paramagnetic state associated with the formation of the $ZnFe_2O_4$ phase, the increase in the heating rate under the external influence of an alternating magnetic field is influenced by Brownian relaxation losses that occur when the grain sizes change and their movement in the solution during exposure to the magnetic field. Moreover, the formation of the paramagnetic $ZnFe_2O_4$ phase leads to an almost 2.5-fold increase in the heating rate in comparison with the same value for nanoparticles containing the magnetite phase. Thus, summing up the assessment of the heating rate of aqueous solutions using Fe_3O_4/ZnO nanoparticles, it can be concluded that composites in which the paramagnetic $ZnFe_2O_4$ phase dominates possess the greatest efficiency in aqueous solution heating. It is also worth to note that in the case of $ZnFe_2O_4$/ZnO nanoparticles, the trend in the *T(t)* dependence is close to linear, while for nanoparticles obtained at annealing temperatures of 100–400°C, a deviation from linearity is observed, indicating a nonadiabatic heat transfer process, which arises as a result of the morphological features of nanoparticles, as well as the presence of inclusions of magnetic disorder.

Fig. 10a–b presents the results of estimates of the specific absorption rate and the power of intrinsic losses, reflecting the dynamics of the heat-conducting properties of nanoparticles when exposed to an alternating magnetic field. These graphs were constructed based on calculated data assessing changes in the heating rate of an aqueous solution under external influence of an alternating magnetic field. Calculations were carried out using formulas (1) and (2). The obtained dependences reflect the efficiency of heat transfer processes and subsequent heating of an aqueous solution by nanoparticles during the time required to heat the solution to 42.5 °C.

The overall appearance of the presented dependence of the change in the SAR value indicates that in the case of Fe_3O_4/ZnO nanoparticles the magnetite and hematite phases are present in the composition, the SAR value is no more than 40–50 W/g, which is a very low indicator reflecting the heating efficiency. Moreover, in addition to low absorption rates, indicating poor heat transfer, the heating time of aqueous solutions using these nanoparticles is quite long, which requires a long exposure time to an alternating magnetic field on living organisms in the case of using these nanoparticles as the basis for hyperthermic studies.

The increase in the efficiency of the specific absorption rate (SAR) and the intrinsic loss power (ILP) observed for $ZnFe_2O_4$ nanoparticles in comparison with Fe_3O_4 in this case can be explained by several factors, including structural features (for $ZnFe_2O_4$ nanoparticles the structural ordering degree is significantly higher), morphological features,

expressed in the fact that $ZnFe_2O_4$ nanoparticles are more uniform in size and particle shape, which excludes the shape effect observed for a mixture of $Fe_3O_4(Fe_2O_3)/ZnO$ particles obtained at annealing temperatures of 100–700 °C. This shape effect is due to the magnetic Fe_3O_4(Fe_2O_3) particles being surrounded by larger ZnO particles, which prevents the rapid heat transfer observed for $ZnFe_2O_4$ particles. In case of non-uniform particle sizes, heat exchange processes will be non-uniform, due to the presence of grain boundaries and defective structure, preventing heat transfer, as a result of which the heating rate will be slower, unlike well-structured, uniform-sized particles. Also, the share of structurally ordered magnetic fraction, the change of which is directly related to the processes of phase formation, plays an important role in the heating processes.

During phase transformations in Fe_3O_4/ZnO nanoparticles associated with the formation of the spinel structure of $ZnFe_2O_4$, leading to a change in the magnetic properties of nanoparticles with the subsequent dominance of paramagnetic behavior, the SAR value increases by more than 2.0–2.5 times, which indicates an increase in efficiency and acceleration of heat transfer processes. At the same time, the dependence of changes in the ILP value for the studied Fe_3O_4/ZnO nanoparticles with variations in their phase composition also indicates an enhancement in the efficiency of heat transfer processes during the formation of the $ZnFe_2O_4$ spinel phase in nanoparticles. In this case, such a difference in the efficiency of heat transfer and heat exchange processes when the phase composition of nanoparticles changes can be explained by the following facts. When the spinel structure of $ZnFe_2O_4$ is formed, the magnetic properties of nanoparticles become characteristic of superparamagnets, which, as a result of external influences by a magnetic field, experience strong vibrations, resulting in changes in the values of Brownian and relaxation losses for nanoparticles, the alteration of which leads to acceleration of heat transfer processes and rapid heating.

Below in Table 2 the results of a comparative analysis of the SAR value efficiency for the studied nanoparticles with literature data taken from a number of works [59–63], reflecting the assessment of the use of various types of nanoparticles as magnetic materials for hyperthermic studies, are presented. According to the analysis, the results obtained for Fe_3O_4/ZnO nanoparticles annealed at 1000 °C, which showed the highest efficiency of use, can compete quite well with other types of iron-containing nanoparticles, including those modified in various ways. Moreover, the proposed method for synthesis of Fe_3O_4/ZnO nanoparticles is less expensive than the methods considered in Refs. [59–63], from which it can be concluded that these nanoparticles are quite promising for using as materials for hyperthermia, taking into account their low cytotoxicity and much higher cell survival compared to $Zn_{1-x}Ca_xFe_2O_4$ nanoparticles [59], for which cell survival was less than 85 %.

4. Conclusion

In this study, using methods of mechanochemical synthesis followed by thermal annealing, the properties and prospects of using Fe_3O_4/ZnO nanoparticles were studied. The use of the mechanochemical synthesis method to obtain nanoparticles makes it possible to scale up this technique for further production of nanoparticles.

Using the X-ray phase analysis method, it was established that the processes of phase transformations occur in two main stages. The first stage consists of the phase transformation $Fe_3O_4 \rightarrow Fe_2O_3$, characteristic of classical transformations of iron oxide upon heating above 400 °C. The second stage is characteristic of the formation of the spinel structure of $ZnFe_2O_4$ with the complete transformation of the Fe_2O_3 phase into $ZnFe_2O_4$, with the replacement of iron ions by zinc ions in octo and tetrahedral positions.

Analysis of the morphological features of synthesized Fe_3O_4/ZnO nanoparticles using scanning electron and transmission electron microscopy methods revealed that variation in the phase composition leads to the enlargement of particles, alongside the formation of agglomerates when $ZnFe_2O_4$ appears in the composition. Moreover, variation in thermal annealing conditions results in the formation of a composite mixture of two types of particles, which are hexagonal particles of zinc oxide surrounded by spherical particles of iron oxide (magnetite or hematite) or $ZnFe_2O_4$.

Using Mössbauer spectroscopy methods, the dependences of the hyperfine parameters of the spectra of iron-containing phases on the annealing temperature were obtained. It has been shown that Fe_3O_4 nanoparticles have a relaxation behavior and represent almost pure maghemite γ-Fe_2O_3, in which, with increasing annealing temperature, the structure improves, and the average sizes of magnetic ordering regions grow. The processes of phase transformations obtained using Mössbauer spectroscopy methods are consistent with the data of X-ray phase analysis.

During assessment of the effectiveness of using synthesized Fe_3O_4/ZnO nanoparticles as a basis for hyperthermic heating of model solutions, it was found that the formation of a spinel structure of the $ZnFe_2O_4$ type results in the solution heating rate growth, and consequently, the application efficiency growth. During the studies, it was found that the formation of the $ZnFe_2O_4$ phase leads not only to an increase in the heating rate, but also to the formation of a linear dependence of the change in the solution temperature on the time of exposure to an alternating magnetic field.

Analysis of the SAR and ILP values for synthesized Fe_3O_4/ZnO nanoparticles showed that the formation of nanoparticles with the dominant $ZnFe_2O_4$ phase in the structure leads to an increase in the efficiency of heat transfer processes by 2.0–2.5 times. These changes are due to effects associated with changes in the vibration processes of nanoparticles in a superparamagnetic state.

CRediT authorship contribution statement

Kamila B. Kaliyekperova: Software, Investigation, Formal analysis, Data curation, Conceptualization. **Vyacheslav S. Rusakov:** Writing – original draft, Visualization, Methodology, Investigation, Formal analysis, Data curation, Conceptualization. **Artem L. Kozlovskiy:** Writing – review & editing, Writing – original draft, Visualization, Supervision, Software, Funding acquisition, Formal analysis, Data curation, Conceptualization. **Maxim S. Fadeev:** Investigation, Formal analysis, Data curation, Conceptualization. **Dmitriy I. Shlimas:** Supervision, Resources, Funding acquisition, Formal analysis, Data curation, Conceptualization. **Maxim V. Zdorovets:** Resources, Methodology, Investigation, Formal analysis, Data curation, Conceptualization.

Table 2
The results of a comparative analysis of the SAR value efficiency for the studied nanoparticles with literature data.

Parameter	Samples					
	Fe_3O_4/ZnO nanoparticles ($T_{annealing}$ – 1000 °C)	$Zn_{1-x}Ca_xFe_2O_4$ nanoparticles [59]	$ZnFe_2O_4$–chitosan-doxorubicin hydrochloride nanoparticles [60]	Fe_3O_4 nanoparticles (NPs) coated with various biocompatible surfactants such as glutamic acid (GA), citric acid (CA), polyethylene glycol (PEG), polyvinylpyrrolidine (PVP), ethylene diamine (EDA) [61]	$CuFe_2O_4$ nanoparticles [62]	Chitosan modified Fe_3O_4 magnetic nanoparticles [63]
SAR, W/g	100.5	60.45	80.66	44–130	44.9	161.16

Informed consent statement

Not applicable.

Institutional review board statement

Not applicable.

Funding

This research was funded by the Ministry of Energy of the Republic of Kazakhstan (No. BR20081011). The work performed by V.S. Rusakov and M.S. Fadeev was supported by the Program for the Development of the Experimental Instrumentation Base of Lomonosov Moscow State University.

Declaration of competing interest

The authors declare that they have no known competing financial interests or personal relationships that could have appeared to influence the work reported in this paper.

Appendix A. Supplementary data

Supplementary data to this article can be found online at https://doi.org/10.1016/j.cscee.2025.101195.

Data availability

No data was used for the research described in the article.

References

[1] P. Guo, et al., Facile synthesis of ZnFe2O4 nanoparticles with tunable magnetic and sensing properties, Langmuir 29 (28) (2013) 8997–9003.
[2] M. Maletin, et al., Synthesis and structural characterization of In-doped ZnFe2O4 nanoparticles, J. Eur. Ceram. Soc. 27 (13–15) (2007) 4391–4394.
[3] M. Mozaffari, M.E. Arani, J. Amighian, The effect of cation distribution on magnetization of ZnFe2O4 nanoparticles, J. Magn. Magn Mater. 322 (21) (2010) 3240–3244.
[4] P.A. Vinosha, et al., Synthesis and properties of spinel ZnFe2O4 nanoparticles by facile co-precipitation route, Optik 134 (2017) 99–108.
[5] M. Bini, et al., Superparamagnetic ZnFe2O4 nanoparticles: the effect of Ca and Gd doping, Mater. Chem. Phys. 204 (2018) 72–82.
[6] N.T.T. Nguyen, et al., Green synthesis of ZnFe2O4 nanoparticles using plant extracts and their applications: a review, Sci. Total Environ. 872 (2023) 162212–162230.
[7] S. Ayyappan, G. Paneerselvam, M.P. Antony, J. Philip, Structural stability of ZnFe2O4 nanoparticles under different annealing conditions, Mater. Chem. Phys. 128 (3) (2011) 400–404.
[8] K. Kombaiah, et al., Studies on Opuntia dilenii haw mediated multifunctional ZnFe2O4 nanoparticles: optical, magnetic and catalytic applications, Mater. Chem. Phys. 194 (2017) 153–164.
[9] Y. Ge, et al., Fabrication and magnetic transformation from paramagnetic to ferrimagnetic of ZnFe2O4 hollow spheres, Trans. Nonferrous Metals Soc. China 29 (7) (2019) 1503–1509.
[10] D.D. Andhare, et al., Structural and chemical properties of ZnFe2O4 nanoparticles synthesised by chemical co-precipitation technique//Journal of Physics: conference series, IOP Publishing 1644 (1) (2020) 12014–12020.
[11] M. Aghazadeh, Zn-doped magnetite nanoparticles: development of novel preparation method and evaluation of magnetic and electrochemical capacitance performances, J. Mater. Sci. Mater. Electron. 28 (2017) 18755–18764.
[12] M.M. Momeni, M. Najafi, Structural, morphological, optical and photoelectrochemical properties of ZnFe2O4 thin films grown via an electrodeposition method, Inorg. Chem. Commun. 132 (2021) 108809–108815.
[13] Z.Ž Lazarević, et al., Nanodimensional spinel NiFe2O4 and ZnFe2O4 ferrites prepared by soft mechanochemical synthesis, J. Appl. Phys. 113 (18) (2013) 187221–187230.
[14] M. Niyaifar, Effect of preparation on structure and magnetic properties of ZnFe 2 O 4, J. Magnet. 19 (2) (2014) 101–105.
[15] Z.Ž. Lazarević, et al., Study of NiFe2O4 and ZnFe2O4 spinel ferrites prepared by soft mechanochemical synthesis//Ferroelectrics 448 (1) (2013) 1–11.
[16] N. Kislov, et al., Optical absorption red and blue shifts in ZnFe2O4 nanoparticles, Mater. Sci. Eng. B 153 (1–3) (2008) 70–77.
[17] F. Hirosawa, et al., Kinetic analysis of mechanochemical reaction for synthesis of zinc ferrite nanoparticles, J. Soc. Powder Technol. 53 (12) (2016) 768–773. Japan.
[18] F. Hirosawa, T. Iwasaki, M. Iwata, Kinetic analysis of mechanochemical reaction between zinc oxide and gamma ferric oxide based on the impact energy and collision frequency of particles, Powder Technol. 352 (2019) 360–368.
[19] A. Nazarova, A.L. Kozlovskiy, V.S. Rusakov, K.B. Egizbek, M.S. Fadeev, B. A. Prmantayeva, K.K. Kadyrzhanov, Study of the applicability of magnetic iron-containing nanoparticles in hyperthermia and determination of their resistance to degradation processes, Crystals 12 (12) (2022) 1816.
[20] P.M. Botta, E.F. Aglietti, J.M.P. López, Kinetic study of ZnFe2O4 formation from mechanochemically activated Zn–Fe2O3 mixtures, Mater. Res. Bull. 41 (4) (2006) 714–723.
[21] J. Deng, C. He, Y. Peng, J. Wang, X. Long, P. Li, A.S. Chan, Magnetic and conductive Fe3O4–polyaniline nanoparticles with core–shell structure, Synth. Met. 139 (2) (2003) 295–301.
[22] J. Deng, C. He, Y. Peng, J. Wang, X. Long, P. Li, A.S. Chan, Magnetic and conductive Fe3O4–polyaniline nanoparticles with core–shell structure, Synth. Met. 139 (2) (2003) 295–301.
[23] H.L. Ding, Y.X. Zhang, S. Wang, J.M. Xu, S.C. Xu, G.H. Li, Fe3O4@ SiO2 core/shell nanoparticles: the silica coating regulations with a single core for different core sizes and shell thicknesses, Chem. Mater. 24 (23) (2012) 4572–4580.
[24] E.C. Abenojar, et al., Structural effects on the magnetic hyperthermia properties of iron oxide nanoparticles, Prog. Nat. Sci.: Mater. Int. 26 (5) (2016) 440–448.
[25] R.D. Raland, J.P. Borah, Efficacy of heat generation in CTAB coated Mn doped ZnFe2O4 nanoparticles for magnetic hyperthermia, J. Phys. Appl. Phys. 50 (3) (2016) 035001.
[26] K. Roumaih, I.A. Ali, S.I. Hussein, Impact of rare earth oxide on ZnFe2O4: structural, magnetic properties, and hyperthermia efficiency, Phys. Scripta 98 (10) (2023) 105941.
[27] S.M. Hoque, et al., Synthesis and characterization of ZnFe2O4 nanoparticles and its biomedical applications, Mater. Lett. 162 (2016) 60–63.
[28] A. Manohar, K. Chintagumpala, K.H. Kim, Magnetic hyperthermia and photocatalytic degradation of rhodamine B dye using Zn-doped spinel Fe 3 O 4 nanoparticles, J. Mater. Sci. Mater. Electron. 32 (2021) 8778–8787.
[29] N.G. Yadav, et al., Impact of collected sunlight on ZnFe2O4 nanoparticles for photocatalytic application, J. Colloid Interface Sci. 527 (2018) 289–297.
[30] R.S. Yadav, et al., Superparamagnetic ZnFe2O4 nanoparticles-reduced graphene oxide-polyurethane resin based nanocomposites for electromagnetic interference shielding application, Nanomaterials 11 (5) (2021) 1112–1120.
[31] V.S. Rusakov, A.L. Kozlovskiy, M.S. Fadeev, K.B. Egizbek, A. Nazarova, K. K. Kadyrzhanov, M.V. Zdorovets, Study of phase transformations and hyperfine interactions in Fe3O4 and Fe3O4@ Au nanoparticles, Nanomaterials 12 (23) (2022) 4121.
[32] M.E. Matsnev, Rusakov V.S. SpectrRelax, An application for Mössbauer spectra modeling and fitting, AIP Conf. Proc. 1489 (1) (2012) 178–185.
[33] S. Kossatz, et al., High therapeutic efficiency of magnetic hyperthermia in xenograft models achieved with moderate temperature dosages in the tumor area, Pharm. Res. 31 (2014) 3274–3288.
[34] P. Kowalik, et al., Yttrium-doped iron oxide nanoparticles for magnetic hyperthermia applications, J. Phys. Chem. C 124 (12) (2020) 6871–6883.
[35] S.S. Pati, et al., Facile approach to suppress γ-Fe2O3 to α-Fe2O3 phase transition beyond 600° C in Fe3O4 nanoparticles, Mater. Res. Express 2 (4) (2015) 045003.
[36] F.S. Yen, et al., Crystallite size variations of nanosized Fe2O3 powders during γ-to α-phase transformation, Nano Lett. 2 (3) (2002) 245–252.
[37] H.T. Hai, et al., Facile synthesis of Fe3O4 nanoparticles by reduction phase transformation from γ-Fe2O3 nanoparticles in organic solvent, J. Colloid Interface Sci. 341 (1) (2010) 194–199.
[38] A.L. Kozlovskiy, et al., Study of phase transformations, structural, corrosion properties and cytotoxicity of magnetite-based nanoparticles, Vacuum (2019) 236–247. T. 163. – C.
[39] Y. Ge, et al., Fabrication and magnetic transformation from paramagnetic to ferrimagnetic of ZnFe2O4 hollow spheres, Trans. Nonferrous Metals Soc. China 29 (7) (2019) 1503–1509.
[40] M. Arias, et al., Synthesis and characterization of magnetic diphase ZnFe2O4/γ-Fe2O3 electrospun fibers, J. Magn. Magn Mater. 323 (16) (2011) 2109–2114.
[41] G. Narsinga Rao, Y.D. Yao, J.W. Chen, Evolution of size, morphology, and magnetic properties of CuO nanoparticles by thermal annealing, J. Appl. Phys. 105 (9) (2009) 093901.
[42] J. Philip, et al., Effect of thermal annealing under vacuum on the crystal structure, size, and magnetic properties of Zn Fe 2 O 4 nanoparticles, J. Appl. Phys. 102 (5) (2007) 054305.
[43] D.H. Jones, K.K.P. Srivastava, Many-state relaxation model for the mossbauer spectra of superparamagnets, Phys. Rev. B 34 (11) (1986) 7542–7548.
[44] E.J.W. Verwey, Electronic conduction of magnetite (Fe_3O_4) and its transition point at low temperatures, Nature 144 (3642) (1939) 327.
[45] J.B. Yang, et al., Magnetic and structural studies of the Verwey transition in $Fe_{3-\delta}O_4$ nanoparticles, J. Appl. Phys. 95 (2004) 7540–7542.
[46] M.S. Fadeev, et al., Iron oxide@gold nanoparticles: synthesis, properties and potential use as anode materials for lithium-ion batteries, Colloids Surf. A Physicochem. Eng. Asp. 603 (2020) 125178.
[47] I.V. Korolkov, et al., Immobilization of carboranes on Fe_3O_4-polymer nanocomposites for potential application in boron neutron cancer therapy, Colloids Surf., A 601 (2020) 125035.
[48] Ligia E. Zamora, et al., Mössbauer and magnetic study of ball milled Fe-doped ZnO Powders, Hyperfine Interact. 232 (2015) 111–118.
[49] L.N. Mahour, et al., Structural, optical and Mössbauer spectroscopic investigations on the environment of Fe in Fe-doped ZnO ($Zn_{1-x}Fe_xO$) ceramics synthesized by

solution combustion method, Ceram. Int. 45 (Issue 18) (2019) 24625–24634. Part A.
[50] J. Grotel, et al., Structure and hyperfine interactions of Fe-doped ZnO powder prepared by Co-precipitation method, Acta Phys. Pol., A 134 (5) (2018) 1048–1052.
[51] H. Ehrhardt, et al., Structural evolution of ball-milled $ZnFe_2O_4$, J. Alloys Compd. 339 (2002) 255–260.
[52] F. Li, et al., Magnetic properties of $ZnFe_2O_4$ nanoparticles produced by a low-temperature solid-state reaction method, J. Magn. Magn Mater. 309 (2007) 295–299.
[53] R.V. Morris, et al., Spectral and other physicochemical properties of submicron powders of hematite (α-Fe_2O_3), maghemite (γ-Fe_2O_3), magnetite (Fe_3O_4), goethite (α-FeOOH), and lepidocrocite (γ-FeOOH)//Geophysical Research, Solid Earth 90 (1985) 3126–3144.
[54] G.M. Costa, et al., The center shift in Mössbauer spectra of maghemite and aluminum maghemites//Clays and Clay Minerals 42 (5) (1994) 628–633.
[55] I.S. Lyubutin, et al., Mössbauer spectroscopy and magnetic properties of hematite/magnetite nanocomposites, J. Appl. Phys. 106 (2009) 034311.
[56] R. Zboril, et al., Iron(III) oxides from thermal processess synthesis, structural and magnetic properties, Mo1ssbauer spectroscopy characterization, and applications, Chem. Mater. 14 (2002) 969–982.
[57] Jessyamma Kurian, M. Jacob Mathew, Structural, optical and magnetic studies of CuFe2O4, MgFe2O4 and ZnFe2O4 nanoparticles prepared by hydrothermal/solvothermal method, J. Magn. Magn Mater. 451 (2018) 121–130.
[58] R. Zamiri, S.A. Salehizadeh, H.A. Ahangar, M. Shabani, A. Rebelo, J.S. Kumar, J.M. F. Ferreira, Optical and magnetic properties of ZnO/ZnFe2O4 nanocomposite, Mater. Chem. Phys. 192 (2017) 330–338.
[59] A. Manohar, V. Vijayakanth, K.H. Kim, Influence of Ca doping on ZnFe2O4 nanoparticles magnetic hyperthermia and cytotoxicity study, J. Alloys Compd. 886 (2021) 161276.
[60] A. Esmaeili, N.A. Hadad, Preparation of ZnFe2O4–chitosan-doxorubicin hydrochloride nanoparticles and investigation of their hyperthermic heat-generating characteristics, Ceram. Int. 41 (6) (2015) 7529–7535.
[61] A. Rajan, M. Sharma, N.K. Sahu, Assessing magnetic and inductive thermal properties of various surfactants functionalised Fe3O4 nanoparticles for hyperthermia, Sci. Rep. 10 (1) (2020) 15045.
[62] S.M. Fotukian, A. Barati, M. Soleymani, A.M. Alizadeh, Solvothermal synthesis of CuFe2O4 and Fe3O4 nanoparticles with high heating efficiency for magnetic hyperthermia application, J. Alloys Compd. 816 (2020) 152548.
[63] M. Jamir, C. Borgohain, J.P. Borah, Chitosan modified Fe3O4 nanoparticles for hyperthermia application, Mater. Today Proc. 65 (2022) 2484–2489.